Intermetallics 157 (2023) 107871

Contents lists available at ScienceDirect

Intermetallics

journal homepage: www.elsevier.com/locate/intermet

Solid-state synthesis, magnetic and structural properties of epitaxial $D0_3$-Fe_3Rh(001) thin films

V.G. Myagkov [a,1], L.E. Bykova [a,*], V.S. Zhigalov [a], A.A. Matsynin [a], S.M. Zharkov [a,b], A.A. Ivanenko [a], G.N. Bondarenko [c], D.A. Velikanov [a]

[a] Kirensky Institute of Physics, Federal Research Center KSC SB RAS, Akademgorodok 50/38, Krasnoyarsk, 660036, Russian Federation
[b] Siberian Federal University, 79 Svobodny pr., Krasnoyarsk, 660041, Russian Federation
[c] Institute of Chemistry and Chemical Technology, Federal Research Center KSC SB RAS, Akademgorodok 50/24, Krasnoyarsk, 660036, Russian Federation

ARTICLE INFO

Keywords:
Thin films
Solid-state synthesis
FeRh alloys
$D0_3$ structure
Magnetic properties
Magnetic anisotropy

ABSTRACT

Here we first report on the formation of epitaxial $D0_3$-Fe_3Rh(001) films grown during solid-state reaction in Rh/Fe(001) bilayers on MgO(001) substrates. Samples of the $Fe_{68}Rh_{32}$ composition above 400 °C showed the formation of a new ordered phase, in addition to the ordered B2–FeRh phase (space group Pm-3m, lattice constant $a = 0.2993$ nm), which becomes the dominant phase in $Fe_{76}Rh_{24}$ samples. These results and the results of the asymmetrical XRD φ-scan prove that the new ordered phase is the ordered $D0_3$-Fe_3Rh(001) phase (space group Fm-3m, lattice constant $a = 0.5888$ nm), forming a cube-on-cube orientation relationship with respect to the MgO(001) substrate. The $D0_3$-Fe_3Rh sample is a soft magnetic material with high saturation magnetization.

1. Introduction

Among Fe_xRh_{100-x} alloys, the alloys close to equatomic ($48 \leq x \leq 56$) composition in both bulk samples and thin films have attracted a great deal of interest in recent years due to their unique first-order metamagnetic transition from an antiferromagnetic α"-phase to a ferromagnetic α'-phase when heated above ~ 370 K [1]. An unusual feature of the reversible α"↔ α' transition is that both phases have an ordered B2 structure and a slight 1% isotropic difference in the lattice constant, which gives existence to the giant magnetostriction [2], large magnetoresistance [3,4] and magnetocaloric effects [5]. This expands the possible use of B2–FeRh thin films for various applications such as heat assisted magnetic recording (HAMR) [6–8], micro-electro-mechanical systems (MEMS) [9] and spintronic devices [10–12]. According to the bulk Fe–Rh phase diagram, the Fe_xRh_{100-x} alloys are not magnetic and have an fcc γ(A1) structure at room temperature when Fe is less than 48 at.% [13,14]. The chemically ordered bcc (B2) structure exists in a wide composition range ($48 \leq x \leq 85$) and at compositions of ($85 \leq x \leq 100$) the alloys are in a chemically disordered bcc (A2) structure [13–16]. Comprehensive high-performance first-principles calculations based on density functional theory predict stable ordered structures of Fe_3Rh (P4/mmm), Fe_2Rh ($C11_b$) and $FeRh_3$ ($D0_{24}$) in the binary Fe–Rh system [17,18] in addition to B2–FeRh. The magnetic moment and anisotropy of Rh_2Fe_m ($m \leq 4$) and ordered $Fe_2Rh(C11_b)$ structures were determined using first-principle calculations based on the Vienna *ab initio* simulation package in ref. 19. The calculations predict the Rh atoms are ferromagnetically coupled to the Fe, the interface Fe moments are about 3.0 μ_B for Rh_2Fe_m and $C11_b$-Fe_2Rh alloys and the largest uniaxial anisotropy is found in Fe_2Rh ($7{\cdot}10^7$ erg/cm^3) [19]. However, the currently known experimental results are often incompatible with theoretical predictions of new phases. It follows from experimental data that, apart from the chemically ordered B2–FeRh phase, there are no other ordered phases in the Fe–Rh system. For many binary alloys, the compositional region of the B2 phase existence is centered near the equiatomic composition. However, in the Fe–Rh system this region is strongly shifted to a region with a high Fe concentration, which suggests the existence of an Fe-rich phase with lattice parameters coinciding or very close to B2–FeRh Back in 1963 G. Shirane et al. [13] expected a $D0_3$ ordering in the Fe-rich part of the Fe–Rh binary. However, efforts to obtain the Fe_3Al type ($D0_3$ structure) ordering in 25 at.% rhodium and 75 at.% iron alloys by cooling from 550 to 300 °C at a rate of 1 °C/h was not successful [13]. Despite numerous studies over the past 60 years, the binary Fe–Rh phase diagram outside the ($48 \leq x \leq 56$) iron composition is still being refined [13,14].

* Corresponding author.
E-mail address: lebyk@iph.krasn.ru (L.E. Bykova).
[1] The author has died.

https://doi.org/10.1016/j.intermet.2023.107871
Received 20 September 2022; Received in revised form 30 January 2023; Accepted 25 February 2023
Available online 2 March 2023

In this paper, we report the investigations of solid-state reaction between polycrystalline Rh and epitaxial Fe(001) films in 32Rh/68Fe (001) and 24Rh/76Fe(001) bilayers with $Fe_{68}Rh_{32}$ and $Fe_{76}Rh_{24}$ atomic ratios, respectively. In both samples, a mixture of epitaxially intergrown $D0_3$-Fe_3Rh(001) and B2–FeRh(001) phases is formed above 400 °C. The lattice parameter, saturation magnetization and the first constant of magnetocrystallographic anisotropy K_1 of the $D0_3$-Fe_3Rh phase were determined. A modified Fe-rich part of the Fe–Rh phase diagram was proposed based on the results obtained in this study.

2. Experimental

Iron-rich 32Rh/68Fe(001) bilayers grown on a MgO(001) substrate were fabricated in two steps. In the first step, the epitaxial Fe(001)/MgO (001) films were grown on single-crystal MgO(001) substrates with a size of 10 × 10 × 1 mm by a thermal evaporation method in a vacuum chamber at a pressure of $1.3{\cdot}10^{-4}$ Pa. To obtain high-quality Fe(001) films, the MgO(001) substrates were previously outgassed at 300 °C for 1 h and the Fe layers were deposited at 250 °C. Epitaxial Fe(001) films had the orientation ratio Fe(001)[100] || MgO(001)[110] with the MgO (001) substrate.

At the second step, a Rh layer was deposited onto the Fe(001)/MgO (001) samples by DC magnetron sputtering. The base pressure of the vacuum chamber was $\sim 1.3{\cdot}10^{-4}$ Pa, the operating pressure was $\sim 1.3{\cdot}10^{-1}$ Pa, in an Ar atmosphere. To prevent a reaction between Rh and Fe, the Rh layer was deposited on Fe(001) at room temperature. Under such deposition conditions the polycrystalline Rh layer was formed on the Fe (001) surface. The thickness of the Fe(001) layer was 150 nm, and the thicknesses of the upper Rh layer was 80 nm for the Rh/Fe(001) bilayers.

To investigate the total elemental composition of the films, analysis was performed by energy-dispersive X-ray spectroscopy (EDS) using a Hitachi TM4000Plus instrument (Tokyo, Japan) equipped with an EDS-detector. EDS analysis was performed in a high vacuum at an acceleration voltage of 20 kV with 100× magnification from a film area of 1.5 mm^2. EDS analysis performed for the initial Rh/Fe(001) bilayers showed the elemental composition of 68 at.% Fe and 32 at.% Rh (Fe68Rh32).

The initial samples were annealed under a vacuum of $1.3{\cdot}10^{-4}$ Pa from room temperature to 800 °C in intervals of 100 °C, holding for 1 h at each temperature. The phase formations and structural changes occurring at the interface between the Rh and Fe layers when the annealing temperature increased, were identified with a DRON-4-07 diffractometer (CuK_α radiation, $\lambda = 0.15406$ nm). The epitaxial film orientations were analyzed by means of asymmetric X-ray diffraction (XRD) scans performed on a PANalytical X'Pert PRO diffractometer (Almelo, The Netherlands) with a PIXcel detector with a PIXcel detector. CuK_α ($\lambda = 0.15406$ nm) radiation monochromatized by a secondary graphite monochromator was used in the instrument. The XRD investigations were carried out using the samples at room temperature.

The saturation magnetization M_S and the coercivity H_C were measured with a vibration sample magnetometer in magnetic fields up to 10 kOe. The constant K_4 in the (001) plane was determined by a torque magnetometer with a sensitivity of $3.76{\cdot}10^{-9}$ Nm in a magnetic field $H = 0$–12 kOe. The saturation magnetization M_S^0 and the magnetic fourfold anisotropy constants K_4^0 were determined for the total volume (V) of the 32Rh/68Fe(001) and 24Rh/76Fe(001) bilayers. All saturation magnetization and the magnetic anisotropy constants measurements were carried out on the samples at room temperature using the torque method presented in Refs. [20,21].

The reversible antiferromagnetic to ferromagnetic (AFM-FM) phase transitions were checked using a Magnetic Properties Measurement System, Quantum Design (MPMS-XL). Magnetic fields of $H = 1.0$ kOe were applied along the in-plane [100] MgO direction which coincides with the easy axis of the Rh/Fe(001) bilayers at all measurements in the 10–450 K temperature interval.

To obtain the films of the Fe_3Rh composition stoichiometry, the single crystal Fe(001) layer of the 75 nm thickness was deposited at a temperature of 200 °C on the $Fe_{68}Rh_{32}$(001) samples, obtained by annealing at 800 °C for 1 h of 32Rh/68Fe(001) bilayers grown on MgO (001), as described above. The EDS analysis showed that the obtained Fe (001)/$Fe_{68}Rh_{32}$(001) samples have an atomic composition of $Fe_{76}Rh_{24}$ (close to the Fe_3Rh composition stoichiometry).

3. Results and discussion

3.1. *Structural and magnetic phase transformations in the 32Rh/68Fe(001) bilayer during annealing up to 800 °C*

Recent studies of solid-state reaction in Rh/Fe(001 bilayers [21] have shown the sequential formation of nonferromagnetic B2 (nfm-B2) at above 100 °C and the ferromagnetic B2-α_l' phase above 300 °C. The B2-α_l' is a modification of the α' phase having a low magnetization about 825 emu/cm^3 and a reversible antiferromagnetic to ferromagnetic (AFM-FM) phase transition that exists in a narrow composition range of nearly equiatomic concentration. It has been shown that in the 45Rh/55Fe(001) bilayers [21], the Fe-rich highly B2-ordered α_h' phase is formed from the equiatomic α_l' compound above 400 °C by the solid-state reaction $\alpha_l' + Fe \rightarrow$ (~450 °C) α_h'. The α_h' phase possessed a magnetization ~1270 emu/cm^3 and the reversible AFM-FM transition was completely suppressed.

In the experiments, we used Fe-rich 32Rh/68Fe(001) bilayers that were grown on a MgO(001) substrate with the atomic composition of $Fe_{68}Rh_{32}$. Fig. 1a shows a schematic diagram of the phase transformations consistently occurring in 32Rh/68Fe(001) bilayers on a MgO (001) substrate during annealing from room temperature to 800 °C, which builds on the X-ray diffraction (XRD) analysis (Fig. 1b) and magnetic measurements (Fig. 1c and d). The transformations consist of the successive formation of a nonferromagnetic B2–FeRh phase (nfm-B2) at above 100 °C in a thin layer at the Rh/Fe interface of the as-deposited sample, which above 300 °C turns into the B2-α_l' phase. Above 500 °C the synthesized $Fe_{68}Rh_{32}$ films contain the highly ordered B2-α_h' (further down in the text B2) and new ordered $D0_3$ phases. The lattice constant of the ordered B2–FeRh phase (space group Pm-3m, lattice constant $a = 0.2993$ nm) is very close to the database data (PDF 4+ card # 01-073-2618, Pm-3m, $a = 0.2987$ nm). In the case of the ordered $D0_3$-Fe_3Rh(001) phase (space group Fm-3m, lattice constant $a = 0.5912$ nm) the crystallographic parameters were experimentally determined for the first time. As shown in Fig. 1b the nfm-B2 and ferromagnetic α_l' phases have very low intensity of the (001) and (002) diffraction reflections, which indicates that both phases epitaxially grow on the Fe(001) surface and both have a chemically ordered B2 nanocrystalline structure. After annealing above 400 °C the intensity of the B2(001) and B2(002) diffraction reflections starts to grow and becomes very strong above 500 °C, which indicates the formation of high structural quality epitaxial B2(001) (B2-α_h') layers on the MgO(001) surface. The phase sequence 32Rh/68Fe → (~100 °C) nfm-B2 → (300 °C) α_l' → (~450 °C) α_h' coincides with the phase sequence in 45Rh/55Fe bilayers [21]. However, above 500 °C, in addition to the superstructural (001) and fundamental (002) reflections from B2 (B2-α_h'), new reflections appear with interplanar spacings $d_{(002)} = 0.2948$ nm and $d_{(004)} = 0.1474$ nm, reflections that belong to a new ordered phase in the Fe-rich region of the Fe–Rh phase diagram. Below, we will show that the new phase has a Fe_3Rh composition and a $D0_3$ ordered Fe_3Al structure. This means that, unlike 45Rh/55Fe(001), which above 500 °C contains only the B2 phase [21], the Fe-rich 32Rh/68Fe(001) bilayers contain a mixture of ordered (B2 + $D0_3$) phases. The intensity of $D0_3$ reflections is well below the intensity from the B2 phase reflections (Fig. 1b), which implies that B2 is the dominant phase after annealing in the range from 600 °C to 800 °C. Fig. 1c shows the dependence of the in-plane relative magnetic anisotropy constant $K_4(T)/K_4^0$ and the relative magnetization $M_S(T)/M_S^0$ as a function of the annealing temperature (T) of the 32Rh/68Fe(001) bilayers, which are similar to the 45Rh/55Fe(001) bilayers [21]. The saturation magnetization $M_S^0 = 1100$ emu/cm^3 and

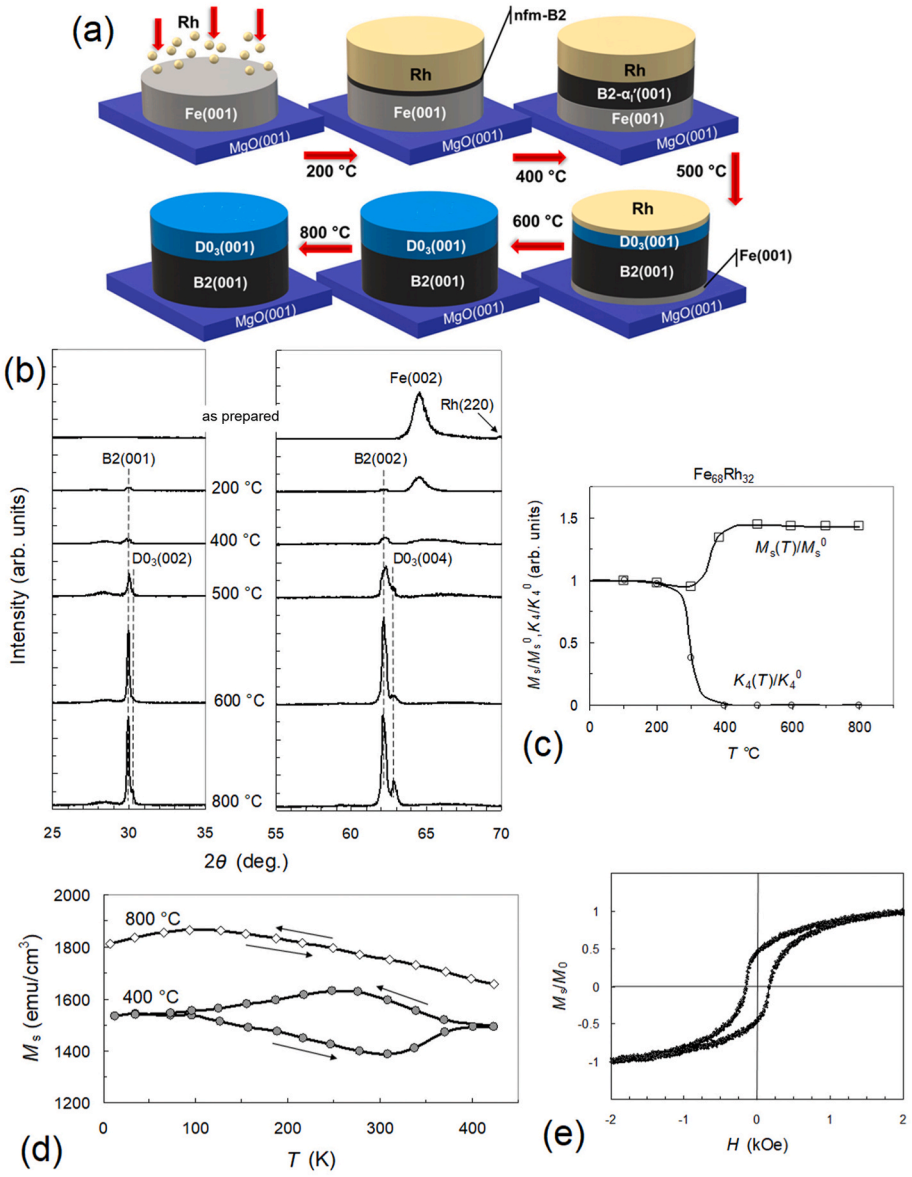

Fig. 1. The synthesis of ordered B2 + D0$_3$ phases in the 32Rh/68Fe(001) bilayer after annealing up to 800 °C. (a) Schematic of the phase transformations in the 32Rh/68Fe(001) bilayer showing the successive formation of the thin non-magnetic nanocrystalline B2–FeRh (nfm-B2) film, which evolves into the low-magnetization modification α$_l$' above 300 °C. After annealing above 400 °C the α$_l$' phase develops into a mixture of α$_h$'(B2) and D0$_3$ phases with high magnetization. (b) XRD patterns of the 32Rh/68Fe(001) bilayer after annealing at different temperatures, indicating the phase transition from the nanocrystalline α$_l$' phase into a mixture of α$_h$'(B2) and D0$_3$ phases with high magnetization above 400 °C. (c) Evolution of the magnetization $M_S(T)/M_S^0$ and anisotropy $K_4(T)/K_4^0$ constants as a function of the annealing temperature. (d) Temperature dependent magnetization curve in 32Rh/68Fe(001) bilayers after annealing at 400 °C and 800 °C. (e) Magnetic hysteresis loop of the Fe$_{32}$Rh$_{68}$ film containing a mixture of the B2 + D0$_3$ phases measured after annealing at 800 °C (M_s^0 ~ 1590 emu/cm^3, H_c ~ 200 Oe, M_r^0 ~ 600 emu/cm^3).

magnetic fourfold anisotropy constant $K_4^0 = 3.1{\cdot}10^5$ erg/cm^3 were determined for the total volume of the 32Rh/68Fe sample. In the temperature range of 500–800 °C, the synthesized Fe$_{68}$Rh$_{32}$ reaction products (B2 + D0$_3$) have a saturation magnetization of ~1590 emu/cm^3 ($M_S(T)/M_S^0$ ~ 1.45), which is significantly higher than ~ 1275 emu/cm^3 of the highly ordered B2 in 45Rh/55Fe(001) samples [21]. This suggests that the magnetization of the D0$_3$ is higher than the magnetization of the B2 phase. The $K_4(T)/K_4^0$ dependence shows that after annealing above 800 °C the magnetic fourfold anisotropy constant K_4(B2 + D0$_3$) ~ 0. The K_4(B2 + D0$_3$) constant contains contributions from the first order magnetocrystallographic anisotropy constants K_1(B2) and K_1(D0$_3$). The value of the K_1(B2) constant of the 45Rh/55Fe(001) samples is close to zero [21], thereby the anisotropy K_1(D0$_3$) constant should be expected to have a low value. Fig. 1d shows the temperature dependent magnetization curve in 32Rh/68Fe(001) bilayers after annealing at 400 °C and 800 °C. The samples show hysteresis of the magnetization in the antiferromagnetic to ferromagnetic (AFM-FM) phase transition, which indicates the existence of a B2-α$_l$' layer in 32Rh/B2-α$_l$'/68Fe(001) films after annealing at 400 °C [21]. However, in the temperature range of 600–800 °C, a mixture of the two (B2 + D0$_3$) phases occurs simultaneously, in which the AFM-FM phase transition is completely suppressed. The magnetic (*M-H*) hysteresis loop after annealing at 800 °C is presented in Fig. 1e, which confirms that the (B2 + D0$_3$) mixture is a soft magnetic material (saturation magnetization M_s^0 ~ 1590 emu/cm^3, coercivity H_c ~ 200 Oe, remanent magnetization M_r^0 ~ 600 emu/cm^3). To summarize, we show the phase evolution in the 32Rh/68Fe(001) bilayer, which like the 45Rh/55Fe(001) bilayer, contains the phase sequence (~100 °C) nfm-B2 → (~300 °C) B2-α$_l$' → (~450 °C) B2-α$_h$', and their only difference is that above 500 °C a new ordered D0$_3$ phase appears in the 32Rh/68Fe films.

3.2. Structural and magnetic properties of the ordered D0$_3$ -Fe$_3$Rh phase

In the experiments, we used Fe(001)/Fe$_{68}$Rh$_{32}$(001) bilayers that were grown on a MgO(001) substrate. To obtain the films of the Fe$_3$Rh composition stoichiometry, a single crystal Fe(001) layer of the 75 nm thickness was deposited on the Fe$_{68}$Rh$_{32}$(001) samples at a temperature of 200 °C. The EDS analysis showed that the obtained Fe(001)/Fe$_{68}$Rh$_{32}$(001) samples have an atomic composition of Fe$_{76}$Rh$_{24}$ (close to the Fe$_3$Rh composition stoichiometry). The process of obtaining the Fe(001)/Fe$_{68}$Rh$_{32}$(001) bilayers is described at the end of Section 2.

Fig. 2a shows a schematic diagram of the phase transformations

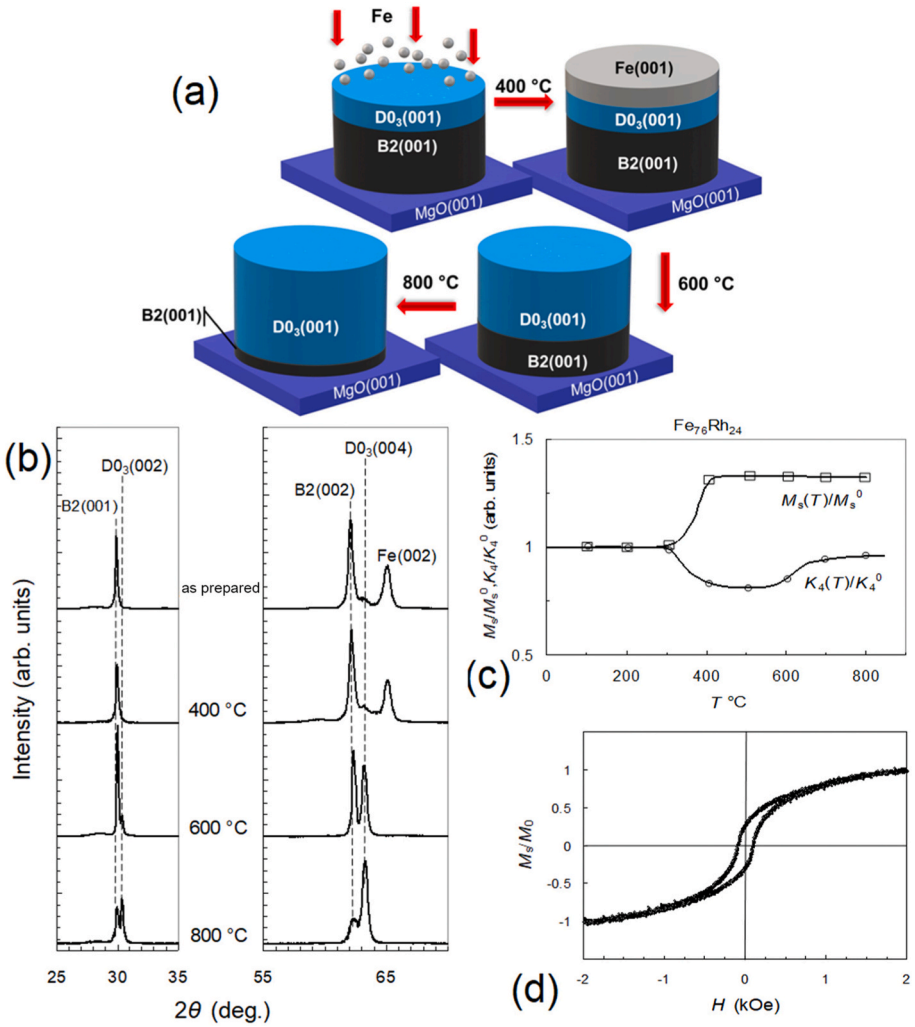

Fig. 2. Formation of the D0$_3$-Fe$_3$Rh(001) basic phase in the Fe(001)/Fe$_{68}$Rh$_{32}$(001) bilayer under annealing up to 800 °C. (a) Schematic of the phase transformations in the Fe(001)/Fe$_{68}$Rh$_{32}$(001) bilayer, showing synthesis of the (B2 + D0$_3$) mixture above 400 °C. (b) XRD patterns of the Fe(001)/Fe$_{68}$Rh$_{32}$(001) bilayer after annealing at different temperatures, indicating that the final reaction products contain a residual B2 phase in addition to the main D0$_3$ phase. (c) Temperature-dependent magnetization $M_S(T)/M_S^0$ and anisotropy $K_4(T)/K_4^0$ constants confirming the synthesis of D0$_3$-Fe$_3$Rh above 400 °C. (d) Magnetic hysteresis loop of the Fe$_{24}$Rh$_{76}$ film measured after annealing at 800 °C (M_s^0 ~ 2150 emu/cm^3, H_c ~ 150 Oe, M_r^0 ~ 540 emu/cm^3).

consistently occurring in Fe(001)/Fe$_{68}$Rh$_{32}$(001) bilayers on a MgO (001) substrate during annealing from 400 °C to 800 °C. The main result is that the basic ordered D0$_3$-Fe$_3$Rh(001) phase is formed in the reaction products above 400 °C, which is epitaxially intergrown with the residual B2(001) phase. Fig. 2b shows XRD patterns of the annealed samples. The original Fe(001)/Fe$_{68}$Rh$_{32}$(001) bilayers contained only reflections from the Fe(001) and Fe$_{68}$Rh$_{32}$(001) layers after annealing at 400 °C. This means that the Fe(001) grew epitaxially in a cube on cube orientation on the mixture of the ordered B2(001) + D0$_3$(001) phases. After annealing at 400 °C, the intensity of the Fe(001) peak decreases and disappears completely above 500 °C. This means that the reaction between Fe(001) and the Fe$_{68}$Rh$_{32}$(001) films ends. In the temperature range 500–800 °C, in contrast to the 32Rh/68Fe(001) samples in which the main B2 phase is formed, the X-ray of the diffraction patterns of the 24Rh/76Fe(001) samples show $d_{(002)}$ = 0.29467 nm and $d_{(004)}$ = 0.14734 nm reflections from the new ordered D0$_3$ phase, which proves that it is the main phase and has Fe$_3$Rh composition. However, the B2 reflections are also present, and they do not disappear with prolonged annealing at 800 °C. This suggests that the final reaction products contain a residual B2 phase in addition to the main D0$_3$ phase. A similar formation of intergrown D0$_3$ and B2 phases was observed in FeGa films [22]. Since the D0$_3$ vol fraction in the Fe$_{76}$Rh$_{24}$ is much larger than in the Fe$_{68}$Rh$_{32}$ samples, it follows that the D0$_3$ structure formation is the result of the solid-state reaction (1) between Fe and B2 which starts above the initiation temperature T_{in} ~ 400°C.

$$Fe + B2\ (\sim 400^{\circ}C) \rightarrow D0_3 \quad (1)$$

Fig. 2c shows the dependence of the in-plane relative magnetic anisotropy constant $K_4(T)/K_4^0$ and the relative magnetization $M_S(T)/M_S^0$ as a function of the annealing temperature (T) of the Fe(001)/Fe$_{68}$Rh$_{32}$(001) films. Both dependencies begin to change after annealing at 400 °C, which is associated with the start of the reaction (1). The values M_S^0 = 1650 emu/cm^3 and $K_4^0 = 0.5 \cdot 10^5$ erg/cm^3 for the Fe(001)/Fe$_{68}$Rh$_{32}$(001) films contain contributions from the magnetizations and anisotropy constants of the Fe(001) and Fe$_{68}$Rh$_{32}$(001) layers, respectively. A rough estimation of the volume fraction of the B2 phase in the (B2+D0$_3$) mixture in the Fe$_{76}$Rh$_{24}$ samples, obtained by calculating the total intensity of the D0$_3$(004) and B2(002) fundamental reflections, does not exceed 10%. Synthesized Fe$_{76}$Rh$_{24}$(001) samples contain the basic D0$_3$ phase after annealing, therefore, neglecting the contribution from the B2 phase, the saturation magnetization M_S(D0$_3$-Fe$_3$Rh) is 2150 emu/cm^3 and the first magnetic anisotropy constant K_1(D0$_3$-Fe$_3$Rh) ~ + $0.5 \cdot 10^5$ erg/cm^3. The constant K_1(D0$_3$-Fe$_3$Rh) was assigned the "+" sign, since the easy axis, as in single-crystal bcc-Fe, coincides with the [100] and [010] directions of the D0$_3$ phase. The K_1(D0$_3$-Fe$_3$Rh) value has a low value, therefore it does not contribute to the magnetic fourfold anisotropy constant K_4 of the synthesized Fe$_{68}$Rh$_{32}$ films. The resulting value M_S (D0$_3$-Fe$_3$Rh) is slightly higher than the values of the Fe$_{75}$Rh$_{25}$ bulk samples (~2000 emu/cm^3), which were obtained in Ref. [13]. Both observations imply that rhodium atoms have a strong effect on increasing the magnetization of the D0$_3$-Fe$_3$Rh phase. Fig. 2d shows the magnetic (M-H) hysteresis loop of the Fe$_{76}$Rh$_{24}$ film after annealing 800 °C which does not saturate at magnetic fields of 2 kOe (saturation

magnetization $M_s^0 \sim 2150$ emu/cm^3, coercivity $H_c \sim 150$ Oe, remanent magnetization $M_r^0 \sim 540$ emu/cm^3). One of the possible reasons for the increase of magnetization at higher fields is a noncollinear alignment of the Fe magnetic moments in the $D0_3$ phase. Thus, soft magnetic $D0_3$-Fe_3Rh with a saturation magnetization of 2150 emu/cm^3 and a magnetic anisotropy constant $K_1 \sim +0.5{\cdot}10^5$ erg/cm^3 is the basic phase in $Fe_{76}Rh_{24}$ films.

3.3. Epitaxial Growth of $D0_3$-Fe_3Rh(001) on MgO(001)

The results of the asymmetrical XRD φ-scan for $Fe_{68}Rh_{32}$ and $Fe_{76}Rh_{24}$, containing reflections after annealing at 800 °C are presented in Fig. 3a,**b**. As is known, many Fe-rich alloys with cubic crystal lattices of 3:1 stoichiometry, such as Fe–Al, Fe–Ga, Fe–Si, Fe–Pd, Fe–Pt and etc. can crystallize into $L1_2$ or $D0_3$ ordered structures. In Fig. 3c, the φ-2θ scans show that only the (00*l*) reflections of B2 and the new phase are visible, along with the (00*l*) reflections of MgO, which indicates that the (001) planes of B2 and the new phase are parallel to the (001) planes of MgO. Previously was shown, using φ-2θ asymmetrical diffraction images, that B2(001)[001] || MgO(001)[110] is the epitaxial orientation for the B2 phases grown by the solid-state reaction between the Rh and Fe(001) layers on the MgO(001) substrate [21]. Asymmetrical φ-scans of the (311) reflection for $L1_2$ (expected lattice constant a = 0.367 nm [13]), and the (112) reflection for $D0_3$ were used to find the orientation relationships and ordering types in the new phases ($D0_3$ or $L1_2$) (Fig. 3c). The φ-scans were carried out using the (311) reflection having no fixed points, which indicates the absence of $L1_2$ ordering in the new phase. Because the new phase has Fe_3Rh composition the φ-scans of the (112) reflection determined that the new phase must have an ordered $D0_3$ crystal structure (space group Fm-3m). Asymmetrical diffraction images on Fig. 3c define the orientation relationship between the $D0_3$-Fe_3Rh film and the MgO substrate, schematically shown in Fig. 3d: $D0_3$(001)[001] || MgO(001)[110]. Lattice parameters were determined for the $Fe_{68}Rh_{32}$ ($\alpha_{B2} = 0.2993$ nm, $\alpha_{D03} = 0.5912$ nm) and $Fe_{76}Rh_{24}$ ($\alpha_{B2} = 0.2980$ nm, $\alpha_{D03} = 0.5888$ nm) samples after annealing at 800 °C.

3.4. Ordered $D0_3$-Fe_3Rh phase and the Fe–Rh phase diagram

The Fe-rich part of the Fe–Rh phase diagram [16] at low temperatures <600 °C contains 0–20 at.% of Rh in the chemically disordered bcc (A2) alloys and between 20 and 50 at.% in the chemically ordered bcc (B2) alloys. At high temperatures above 600 °C only the chemically disordered fcc (A1) alloys and paramagnetic B2 exist in the concentration range of 0–50 at.% Rh. Fig. 4 shows the modified Fe-rich part of the Fe–Rh phase diagram based on the experimental results of this work. The region of the phase mixture of ($D0_3$ + B2) is limited by the compositions of $Fe_{76}Rh_{24}$ and $Fe_{68}Rh_{32}$. However, the real ($D0_3$ + B2) region can be much wider, since the phase boundaries A2/($D0_3$ + B2) and ($D0_3$ + B2)/B2 have not been strictly found. The characteristic temperature 400 °C was also detected for the ($D0_3$ + B2) region by magnetic measurements (Figs. 1c and 2c).

For many film systems, it has been shown that the initiation temperature T_{in} of solid-state reaction in A/B bilayers starts at the temperature of phase transformations T_k in A-B binary system (see for example [21–27] and the references therein for more details about this topic). Consequently, the equality $T_{in} = T_k$ can be used to analyze the phase equilibrium diagrams. This implies that the study of reaction in A/B bilayers with different layer ratios is the study of the A-B phase diagram as the temperature increases from room temperature to high temperatures (bottom-up approach). This approach differs from the generally

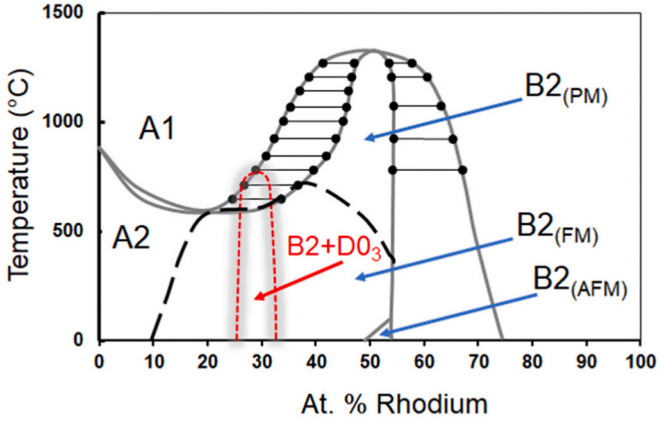

Fig. 4. Modified phase diagram of an Fe–Rh system adapted from ref. 16. Revised Fe-rich part of the Fe–Rh phase diagram contains a new B2+$D0_3$ region. The real B2+$D0_3$ region can be wider, since the phase boundaries A2/B2+$D0_3$ and B2/B2+$D0_3$ are not precisely defined.

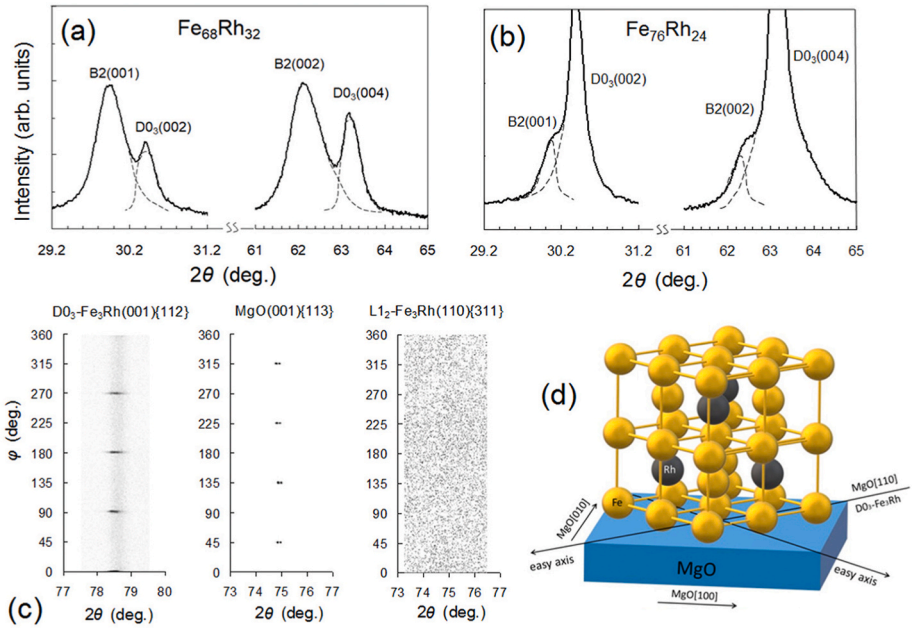

Fig. 3. Epitaxial growth of the $D0_3$(001) phase on MgO(001). (a, b) - XRD scans of epitaxial $Fe_{68}Rh_{32}$ and $Fe_{76}Rh_{24}$ films after annealing at 800 °C. (c) The φ-2θ asymmetric diffraction images for the $Fe_{76}Rh_{24}$(001) film and MgO(001) substrate. These scans prove that the new phase derives a $D0_3$ ordering in the $Fe_{76}Rh_{24}$ film and reveals the $D0_3$(001)[100] || MgO(001)[110] epitaxial orientation relationship. (d) Schematic drawing illustrating the epitaxial relationship of the $D0_3$(001) on the MgO(001) substrate and the locations of the easy axes.

accepted construction of the equilibrium phase diagram of binary metallic systems by cooling the melt to room temperature (top-down approach). Therefore, the temperature hysteresis of the phase formation is possible at a given concentration via both approaches. As argued above, it is assumed that the initiation temperature of solid-state reaction (1) $T_{in} = 400$ °C coincides with the temperature of the unknown phase transformation in the Fe–Rh system. The bulk phase diagram for Fe–Rh above 600 °C contains an A1 phase with an fcc structure, however, A1 is not observed in the $Fe_{76}Rh_{24}$ and $Fe_{68}Rh_{32}$ compositions up to 800 °C. We believe that the bottom-up approach suggests the formation of the A1 phase occurs at temperatures above 800 °C. Thus, additional studies are needed to refine the phase boundaries of the $D0_3$ + B2 region and the high-temperature part of the Fe-rich part of the Fe–Rh phase diagram.

4. Conclusions

In summary, we have discovered a new ordered $D0_3$-Fe_3Rh phase, using a solid-state reaction between epitaxial Fe(001) and polycrystalline Rh layers. The epitaxially intergrown mixture of the $D0_3$(001) + B2(001) phases grows epitaxially on the MgO(001) substrate in both 32Rh/68Fe(001) and 24Rh/76Fe(001) bilayers above 400 °C. The high structural perfection of the ordered $D0_3$(001) and B2 (001) phases obtained by this method makes it possible to separate close reflections from the $D0_3$-Fe_3Rh and B2–FeRh phases. The lattice parameter $\alpha_{D03} = 0.5888$ nm, the saturation magnetization M_S($D0_3$-Fe_3Rh) ~ 2150 emu/cm^3 and the first magnetic anisotropy constant K_1($D0_3$- Fe_3Rh) ~ + 0.5·10^5 erg/cm^3 were determined for the $D0_3$-Fe_3Rh phase. Thus, our work not only justified a method for finding the ordered $D0_3$-Fe_3Rh (001) phase, but also suggests that this method can be extended for iron-based alloys to find ordered $D0_3$ structures in which $D0_3$ has closely spaced X-ray diffraction reflections with A2 and B2 phases.

CRediT authorship contribution statement

All authors contributed to the manuscript and the interpretation of the data.

Author statement

All authors acknowledge that the material presented in this manuscript has not been previously published, nor is it simultaneously under consideration by any other journal.

Declaration of competing interest

The authors declare that they have no known competing financial interests or personal relationships that could have appeared to influence the work reported in this paper.

Data availability

No data was used for the research described in the article.

Acknowledgements

The authors are grateful to L.A. Solovyov for carrying out the XRD φ-scan experiments and I.V. Nemtsev for the measurements of the sample composition. The work is partially based upon the experiments performed at Krasnoyarsk Regional Center of Research Equipment of Federal Research Center « Krasnoyarsk Science Center SB RAS». This research did not receive any specific grant from funding agencies in the public, commercial, or not-for-profit sectors.

References

[1] L.H. Lewis, C.H. Marrows, S. Langridge, Coupled magnetic, structural, and electronic phase transitions in FeRh, J. Phys. D Appl. Phys. 49 (2016), 323002, https://doi.org/10.1088/0022-3727/49/32/323002.
[2] M.R. Ibarra, P.A. Algarabel, Giant volume magnetostriction in the FeRh alloy, Phys. Rev. B 50 (1994) 4196–4199, https://doi.org/10.1103/PhysRevB.50.4196.
[3] I. Suzuki, T. Naito, M. Itoh, T. Sato, T. Taniyama, Clear correspondence between magnetoresistance and magnetization of epitaxially grown ordered FeRh thin films, J. Appl. Phys. 109 (2011), 07C717, https://doi.org/10.1063/1.3556754.
[4] X.Z. Chen, J.F. Feng, Z.C. Wang, J. Zhang, X.Y. Zhong, C. Song, L. Jin, B. Zhang, F. Li1, M. Jiang, Y.Z. Tan, X.J. Zhou, G.Y. Shi, X.F. Zhou, X.D. Han, S.C. Mao, Y. H. Chen, X.F. Han, F. Pan, Tunneling anisotropic magnetoresistance driven by magnetic phase transition, Nat. Commun. 8 (2017) 449, https://doi.org/10.1038/s41467-017-00290-4.
[5] S.A. Nikitin, G. Myalikgulyev, A.M. Tishin, M.P. Annaorazov, K.A. Asatryan, A. L. Tyurin, The magnetocaloric effect in Fe49Rh51 compound, Phys. Lett. 148 (1990) 363–366, https://doi.org/10.1016/0375-9601(90)90819-A.
[6] J.-U. Thiele, S. Maat, E.E. Fullerton, FeRh/FePt exchange spring films for thermally assisted magnetic recording media, Appl. Phys. Lett. 82 (2003) 2859–2861, https://doi.org/10.1063/1.1571232.
[7] Y. Jiao, Z. Liu, R.H. Victora, Renormalized anisotropic exchange for representing heat assisted magnetic recording media, J. Appl. Phys. 117 (2015) 17E317, https://doi.org/10.1063/1.4916184.
[8] R.F. Need, J. Lauzier, L. Sutton, B.J. Kirby, J. de la Venta, Using structural phase transitions to enhance the coercivity of ferromagnetic films, Apl. Mater. 7 (2019), 101115, https://doi.org/10.1063/1.5118893.
[9] S. Hashi, S. Yanase, Y. Okazaki, M. Inoue, A large thermal elasticity of the ordered FeRh alloy film with sharp magnetic transition, IEEE Trans. Magn. 40 (2004) 2784–2786, https://doi.org/10.1109/TMAG.2004.832445.
[10] I. Suzuki, Y. Hamasaki, M. Itoh, T. Taniyama, Controllable exchange bias in Fe/metamagnetic FeRh bilayers, Appl. Phys. Lett. 105 (2014), 172401, https://doi.org/10.1063/1.4900619.
[11] S. Zhang, S. Xia, Q. Cao, D. Wang, R. Liu, Y. Du, Observation of topological Hall effect in antiferromagnetic FeRh film, Appl. Phys. Lett. 115 (2019), 022404, https://doi.org/10.1063/1.5099183.
[12] Z. Feng, H. Yan, Z. Liu, Electric-field control of magnetic order: from FeRh to topological antiferromagnetic spintronics, Adv. Electron. Mater. 5 (2019), 1800466, https://doi.org/10.1002/aelm.201800466.
[13] G. Shirane, C.W. Chen, P.A. Flinn, R. Nathans, Mössbauer study of hyperfine fields and isomer shifts in the Fe-Rh alloys, Phys. Rev. 131 (1963) 183–190. https://journals.aps.org/pr/pdf/10.1103/PhysRev.131.183.
[14] I. Ohnuma, T. Gendo, R. Kainuma, G. Inden, K. Ishida, Phase equilibria and thermodynamic evaluation approximating short-range ordering energy in the Fe–Rh binary system, ISIJ Int. 49 (2009) 1212–1219, https://doi.org/10.2355/isijinternational.49.1212.
[15] T. Usami, M. Itoh, T. Taniyama, Compositional dependence of Gilbert damping constant of epitaxial $Fe_{100-x}Rh_x$ thin films, Appl. Phys. Lett. 115 (2019), 142403, https://doi.org/10.1063/1.5120597.
[16] J. Ye, M. Hauke, V. Singh, R. Rawat, M. Gupta, A. Tayal, S.M. Amir, J. Stahne, A. Paul, Magnetic properties of ordered polycrystalline FeRh thin films, RSC Adv. 7 (2017) 44097–44103, https://doi.org/10.1039/c7ra06738k.
[17] O. Levy, R.V. Chepulskii, G.L.W. Hart, S. Curtarolo, The new face of rhodium alloys: revealing ordered structures from first principles, J. Am. Chem. Soc. 132 (2010) 833–837, https://doi.org/10.1021/ja908879y.
[18] G.L.W. Hart, S. Curtarolo, T.B. Massalski, O. Levy, Comprehensive search for new phases and compounds in binary alloy systems based on platinum-group metals, using a computational first-principles approach, Phys. Rev. X 3 (2013), 041035, https://doi.org/10.1103/PhysRevX.3.041035.
[19] A. Kashyap, R. Skomski, P. Manchanda, J.E. Shield, D.J. Sellmyer, Layered transition-metal permanent-magnet structures, J. Appl. Phys. 109 (2011), 07A714, https://doi.org/10.1063/1.3556766.
[20] S. Chikazumi, Epitaxial growth and magnetic properties of single-crystal films of iron, nickel, and permalloy, J. Appl. Phys. 32 (1961) S81–S82, https://doi.org/10.1063/1.2000506.
[21] V.G. Myagkov, A.A. Ivanenko, L.E. Bykova, V.S. Zhigalov, M.N. Volochaev, D. A. Velikanov, A.A. Matsynin, G.N. Bondarenko, Solid-state synthesis, magnetic and structural properties of interfacial B2-FeRh(001) layers in Rh/Fe(001) films, Sci. Rep. 10 (2020), 10807, https://doi.org/10.1038/s41598-020-67837-2.
[22] V.G. Myagkov, L.E. Bykova, V.S. Zhigalov, D. Kokh, YuL. Mikhlin, A.A. Matsynin, G.N. Bondarenko, Solid-State synthesis, structural and magnetic characterization of ferromagnetic phases in 24Ga/76Fe(001), 40Ga/60Fe(001) and 60Ga/40Fe(001) bilayers, JMMM 561 (2022), 169709, https://doi.org/10.1016/j.jmmm.2022.169709.
[23] V.G. Myagkov, L.E. Bykova, V.S. Zhigalov, A.A. Matsynin, D.A. Velikanov, G. N. Bondarenko, Solid-state synthesis, rotatable magnetic anisotropy and characterization of $Co_{1-x}Pt_x$ phases in 50Pt/50fccCo(001) and 32Pt/68fccCo(001) thin films, J. Alloys Compd. 861 (2021), 157938, https://doi.org/10.1016/j.jallcom.2020.157938.
[24] V.G. Myagkov, L.E. Bykova, A.A. Matsynin, M.N. Volochaev, V.S. Zhigalov, I. A. Tambasov, YuL. Mikhlin, D.A. Velikanov, G.N. Bondarenko, Solid state synthesis of Mn_5Ge_3 in Ge/Ag/Mn trilayers: structural and magnetic studies, J. Solid State Chem. 246 (2017) 379–387, https://doi.org/10.1016/j.jssc.2016.12.010.
[25] V.G. Myagkov, L.E. Bykova, V.S. Zhigalov, A.A. Matsynin, D.A. Velikanov, G. N. Bondarenko, Phase formation sequence, magnetic and structural development

during solid-state reactions in epitaxial 72Pt/28fcc-Co(001) thin films, J. Alloys Compd. 706 (2017) 447–454, https://doi.org/10.1016/j.jallcom.2017.02.261.

[26] V. Myagkov, O. Bayukov, Y. Mikhlin, V. Zhigalov, L. Bykova, G. Bondarenko, Long-range chemical interactions in solid-state reactions: effect of an inert Ag interlayer on the formation of $L1_0$-FePd in epitaxial Pd(001)/Ag(001)/Fe(001) and Fe(001)/Ag(001)/Pd(001) trilayers, Phil. Mag. 94 (2014) 2595–2622, https://doi.org/10.1080/14786435.2014.926037.

[27] V.G. Myagkov, V.S. Zhigalov, A.A. Matsynin, L.E. Bykova, YuL. Mikhlin, G. N. Bondarenko, G.S. Patrin, G.Yu Yurkin, Formation of ferromagnetic germanides by solid-state reactions in 20Ge/80Mn films, Thin Solid Films 552 (2014) 86–91, https://doi.org/10.1016/j.tsf.2013.12.029.